Research Article

Qian Zhang#, Jun-Jun Wang#, Qian Xue, Ying-Jie Wang, Min Zhang*, and Yong-Jin Chen*

Improved osseointegration of dental titanium implants by TiO_2 nanotube arrays with self-assembled recombinant IGF-1 in type 2 diabetes mellitus rat model

https://doi.org/10.1515/ntrev-2023-0120
received December 5, 2022; accepted August 21, 2023

Abstract: Improvement of poor implant osseointegration under diabetes is always a poser in clinics. The purpose of this study was to investigate the effect of TiO_2 nanotubes (TNTs) and self-assembled minTBP-1-IGF-1 on implant osseointegration in type 2 diabetes mellitus (T2DM) rats. There were four groups, the control group, the TNTs group, the minTBP-1-IGF-1 group, and the minTBP-1-IGF-1-TNTs group. The atomic force microscopy and scanning electron microscope (SEM) results showed that 500 nm nanotubes were formed by anodic oxidation and minTBP-1-IGF-1 could self-assemble into almost all nanotubes. ELISA assay confirmed that more protein was adsorbed on TNTs surface. The contact angle of the minTBP-1-IGF-1-TNTs group was the lowest, confirmed that the hydrophilicity was the highest. The double fluorescence staining was used to evaluate the mineral apposition rate (MAR) at early stage and the MAR of the minTBP-1-IGF-1-TNTs group was the highest. Micro-CT images displayed that bone formed around the minTBP-1-IGF-1-TNTs implant was the most homogeneous and dense, and the quantitative analysis of these images at 12 weeks also confirmed these results. The cross-section SEM results showed that the connection between bone and minTBP-1-IGF-1-TNTs implant was the tightest. All results demonstrated that minTBP-1-IGF-1-TNTs can significantly improve low implant osseointegration under T2DM condition.

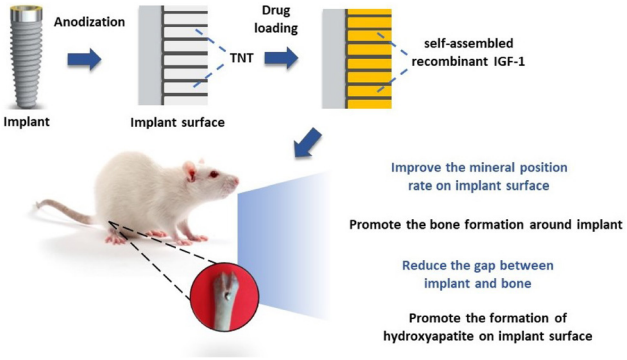

Graphical abstract

Keywords: nanotube, osseointegration, implant, T2DM, peptide aptamer

1 Introduction

Implants have been used to replace missing teeth by achieving stability through close contact with bone (osseointegration), therefore bone quality and quantity around implant are particularly important [1,2]. However, in some pathological conditions, such as diabetic patients, the osseointegration may be impaired because of the poor bone quality and quantity [3]. Diabetes mellitus (DM) is characterized by high concentration of blood glucose, and type 2 diabetes mellitus (T2DM) accounts for about 90–95% of all diagnosed cases of DM [4]. T2DM is

# These authors contributed equally to this work and should be considered first co-authors.

* **Corresponding author: Min Zhang,** State Key Laboratory of Oral & Maxillofacial Reconstruction and Regeneration & National Clinical Research Center for Oral Diseases & Shaanxi International Joint Research Center for Oral Diseases, Department of General Dentistry and Emergency, School of Stomatology, Air Force Medical University, Xi'an 710032, China, e-mail: cherryzhangmin@126.com
* **Corresponding author: Yong-Jin Chen,** State Key Laboratory of Oral & Maxillofacial Reconstruction and Regeneration & National Clinical Research Center for Oral Diseases & Shaanxi International Joint Research Center for Oral Diseases, Department of General Dentistry and Emergency, School of Stomatology, Air Force Medical University, Xi'an 710032, China, e-mail: cyj1229@fmmu.edu.dn
Qian Zhang, Jun-Jun Wang, Qian Xue, Ying-Jie Wang: State Key Laboratory of Oral & Maxillofacial Reconstruction and Regeneration & National Clinical Research Center for Oral Diseases & Shaanxi International Joint Research Center for Oral Diseases, Department of General Dentistry and Emergency, School of Stomatology, Air Force Medical University, Xi'an 710032, China

currently one of the most common systemic diseases affecting implant therapy [3]. T2DM individuals may have reduction in differentiation and proliferation of osteoblasts, which in turn can weaken the expression of bone-matrix genes and cripple production of new bone [5–8].

The latest progress in surface modification of implants is believed to improve bone integration in patients with metabolic disorders, which can impair bone healing [9]. The surface modification can increase bone formation around implant [10]. In recent years, TiO_2 nanotubes (TNTs) prepared through anodic oxidation have attracted much attention as they simulate the basic nanoscale structure of bone and exhibit excellent biocompatibility and osseointegration ability [11]. Several studies have confirmed that Ti specimens modified by TNTs exhibit improved cell adhesion and proliferation ability, alkaline phosphatase activity, and bone mineralization [12]. Meanwhile, recent studies have attempted to use TNTs for drug delivery and local administration. Drugs along with TNTs represent an emerging new trend in implantable therapeutics [13].

TNTs have been extensively explored owing to their fainter *in vivo* immunogenicity, easy preparation, highly controllable topography, mechanical stiffness, chemical resistivity, high loading capability, and eminent surface-to-volume ratio [14–16]. To date, a lot of studies have concentrated on loading hollow TNTs with various therapeutic drugs such as, bone morphogenetic protein 2, metformin, paclitaxel, and vancomycin [17–19]. Insulin-like growth factors 1 (IGF-1), which is considered to participate in the regulation of blood glucose and play a central role in bone remodeling, is produced and reserved in bone matrix [12]. Furthermore, IGF-1 can adjust bone formation and remodeling by influencing the survival and proliferation of osteoblasts [20–22]. In this study, we use protein recombination technology to integrate TiO_2 aptamer minTBP-1 with IGF-1, which not only can self-assemble into TNTs but also possess the therapeutic effect of improving bone quality. MinTBP-1 (RKLPDA), a novel peptide aptamer, has been affirmed to possess the high affinity with TiO_2, which can connect with TiO_2 like a “glue” to introduce bioactive molecules [23–25]. In order to effectively carry the macromolecular protein IGF-1, we connected three minTBP-1 to the N-terminal of IGF-1 [26], which can automatically self-assemble into TNTs.

In this study, TNTs arrays were formed on dental implant surface by anodic oxidation, and these TNTs provided empty spaces for self-assembled minTBP-1-IGF-1 loading. The effects of TNTs and minTBP-1-IGF-1 on bone-implant osseointegration were investigated in T2DM rats.

2 Materials and methods

2.1 Materials processing and surface characterization

Cylindrical screwed Ti implants (1.5 mm^2 × 3.5 mm, Zhong Bang Corporation, Xi’an, China) were divided into four groups: the control group (machined surface), the TNTs group, the minTBP-1-IGF-1 group, and the minTBP-1-IGF-1-TNTs group. All samples were ultrasonically washed with acetone, ethyl alcohol, and deionized water for 30 min sequentially. For TNTs array, Ti implants were anodized at 10 V for 60 min in an electrolyte solution consisting of HF:H_2O at a ratio of 1:99 wt %. Then these samples were washed with deionized water followed by a gentle ultrasonication and sterilized under ethylene oxide. For minTBP-1-IGF-1 self-assembling, machined implants or anodized implants were completely covered by the minTBP-1-IGF-1 solution with a concentration of 1 μg/mL for 6 h at room temperature [15]. Morphological features were characterized by an atomic force microscopy (AFM, Vecco Instrument Dimension, Icon) and field emission scanning electron microscope (FE-SEM, JEOL JSM-6460).

2.2 Water contact angle test

The surface hydrophilicity was measured by contact angle measurements employing Automatic Contact Angle Meter Model SL200B (Solon, Shanghai, China) at room temperature. The test was conducted on a flat surface of the upper part of the implant. Droplet volume is 1 μL.

2.3 Assaying adsorbed modified IGF-1s

The adsorbed amount of minTBP-1-IGF-1 was quantified applying a Human IGF-1 ELISA development kit (PeproTech, Rocky Hill, NJ). To measure the amount of adsorbed protein, specimens were submerged into protein solution for 30 min, 1, 6, and 24 h at room temperature. Then the specimens were introduced into 5 M urea, 0.2 M HCl, and 0.1% Tween-20 for 30 min. This eluate was deliquated 1:20 in PBS containing 0.1% BSA before implementing ELISAs.

2.4 Animal model of type 2 diabetes, intraperitoneal glucose tolerance test (IPGTT), and insulin tolerance test (ITT)

The design and implementation of the experiment were consented by the Animal Ethics Committee of Air Force

Medical University (052/2019) and reported according to the ARRIVE guidelines with respect to relevant items [27]. The male Sprague-Dawley (SD) rats (260–300 g, 9 weeks old) were purchased from the animal holding center of the university. As per previous research, a high-carbohydrate–high-fat diet (comprising 48% carbohydrate, 20% protein, and 22% fat, with total calories of 44.3 kJ/kg) and low-level (30 mg/kg) streptozotocin intraperitoneal injection were implemented into 24 SD rats to elicit T2DM [28].

During the experiment, the weight of rats was measured and the weight changes of normal rats and T2DM rats were compared.

For IPGTT, rats were fasted overnight for 15 h, and were administered with glucose load (1.5 g/kg) through IP injection. Blood was collected from the tail vein for glucose measurements at 0, 10, 20, 30, 60, 90, and 120 min after glucose injection and calculated the area under the curve (AUC) [29].

For ITT, rats were fasted overnight for 15 h. The same cohort of rats were injected with insulin at a dose of 2.5 U/kg bw i.p. and then blood was drawn from the tail vein for glycemia measurements at 0, 15, 30, 60, and 120 min after insulin administration and calculated the AUC.

The body weight, IPGTT, and ITT of six normal rats were measured for comparison with the T2DM rats.

2.5 *In vivo* implantation

Each rat was anaesthetized with diazepam and pentobarbitalnatrium. Four kinds of implants were implanted into T2DM rat distal femurs at random (Figure 1). After surgery, penicillin was injected daily at a dose of 4 WU/kg for 5 days.

2.6 Measurement of mineral apposition rate (MAR)

T2DM rats were subcutaneously injected with tetracycline (15 mg/kg, Sigma, USA) and calcein (10 mg/kg, Sigma) at 4 and 8 weeks after implantation. After execution, samples were cleaned of soft tissue and fixed in 70% ethanol, then dehydrated and embedded with acrylic resin. The hard tissue embedded block was properly trimmed and sectioned with a slicer (Leica 2500e, Leica Company). Three slices were obtained for each sample. There were six slices per group. Then, 10 μm thick hard tissue sections were observed under an E-800 fluorescent microscope (Nikon). The ImagePro Plus analysis system was applied to measure the distance between the two labeled fluorescence lines. A grid of crosses was laid over the image and where a grid point met one of the fluorescent bands, the distance was measured from that point to the nearest point on the next band. A minimum of ten measurements were recorded for each slice, and the final value was an average of these measurements. The MAR was calculated by dividing the distance between the two labels by the interlabeling period in days [5].

2.7 Longitudinal, *in vivo* micro-CT evaluation

Micro-CT (Inveon, Siemens, Germany; 80 kV, 500 μA, 900 ms integration time) scanning at a resolution of 21 μm was performed after anesthesia in T2DM rats at 4, 8, and 12 weeks after implantation. The scanning area included bone within a radius of 1.5 mm with the implant midline as the axis. Bone volume/total volume (BV/TV), trabecular thickness (Tb.Th), trabecular number (Tb.N), bone surface/bone volume (BS/BV), and trabecular separation (Tb.Sp) were determined.

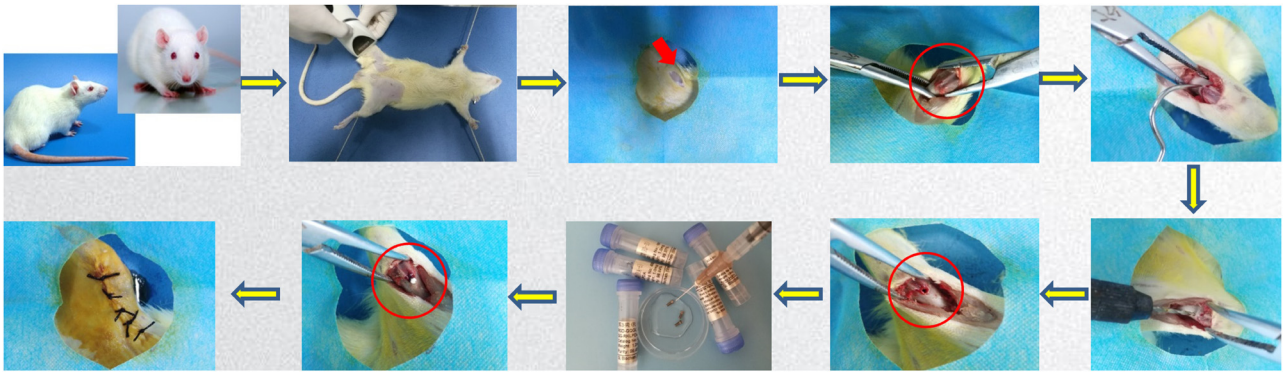

Figure 1: Procedure of implantation surgery.

2.8 SEM/energy dispersive spectrometer (EDS) analysis of cross-sections

Few specimens of each group were embedded in acrylic resin, and then intersected intermediately. The cross-section surfaces were characterized by SEM/EDS. The EDS analysis results were only used for qualitative analysis.

2.9 Statistical analysis

The data were expressed as mean ± standard deviation and subjected to normality testing. The statistical significance of differences was determined by one-way analysis of variance and Tukey's multiple comparison tests using SPSS 16.0 statistical software. Probabilities of less than 0.05 were accepted as significant.

3 Results and discussion

3.1 Surface characterization

To study the surface topography, the interface was analyzed by AFM and SEM. The control group exhibited a coarse surface, many gullies (Figure 2(a), (b), and (i)). After protein adsorption, Ti surface was almost covered by protein, but the adsorbed protein on Ti was uneven (Figure 2(e), (f), and (j)). The AFM images (Figure 2(c) and (d)) of the TNTs samples presented uniformly distributed nano-protrusions; the SEM images (Figure 2(k)) revealed that the highly ordered TNTs were achieved and the nanotubes' diameter was about 500 nm. The nanotube windows were clean and open. When minTBP-1-IGF-1 was loaded, it can be seen from Figure 2(l) that the fusion protein self-assembled into almost every nanotube. And it demonstrated that the nano-

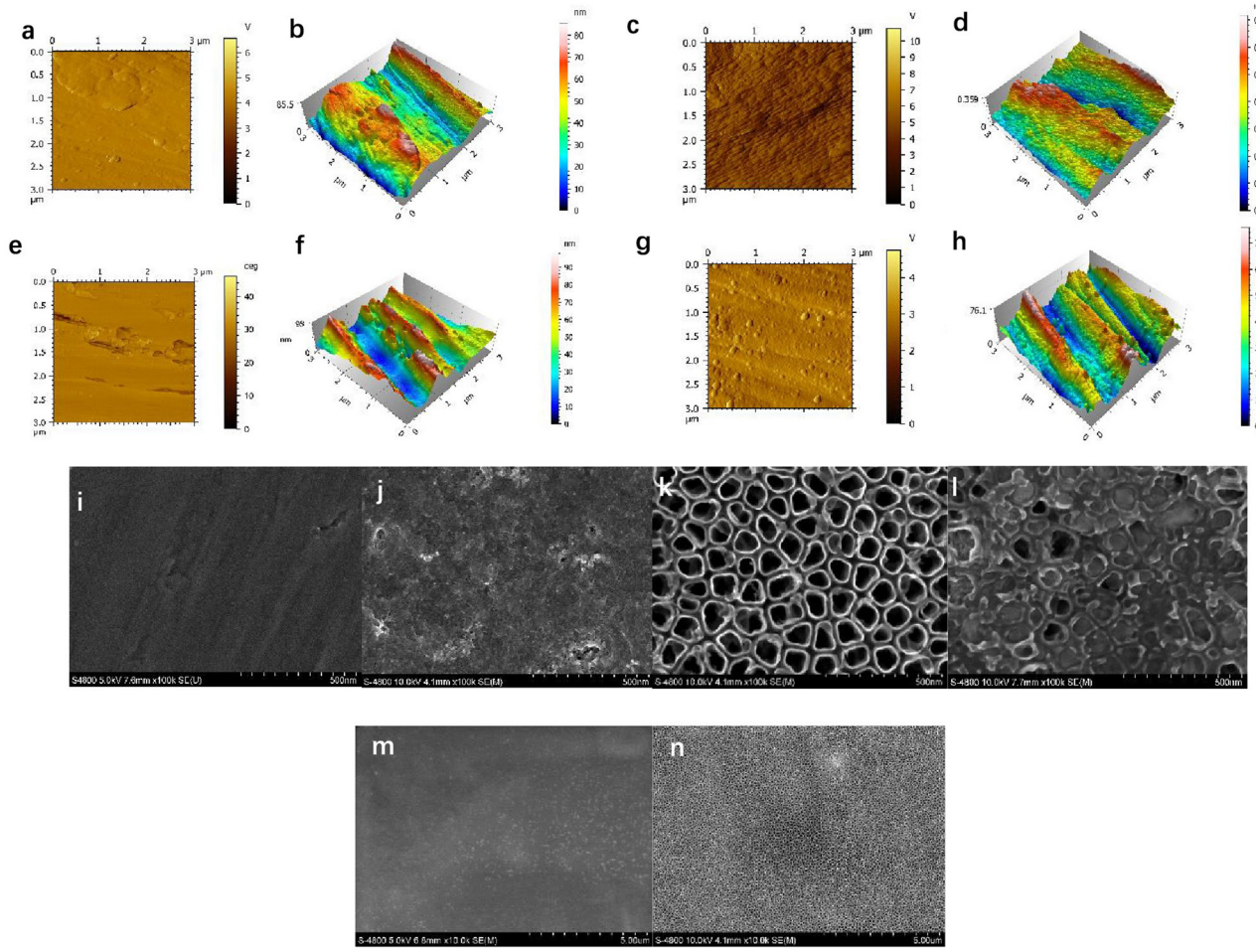

Figure 2: Surface characterization of the modified implant surface: (a) and (b) AFM images of the machined surface, (c) and (d) AFM images of the TNTs surface, (e) and (f) AFM images of the minTBP-IGF-1 surface, (g) and (h) AFM images of the minTBP-1-IGF-1-TNTs surface, (i)–(l) SEM images of the machined, minTBP-1-IGF-1, TNTs, and minTBP-1-IGF-1-TNTs surface (scale bars: 500 nm), and (m) and (n) SEM images of TNTs and minTBP-1-IGF-1-TNTs (scale bars: 5 μm).

Table 1: Ra values of surface roughness of the four experimental groups

Group	Ra (nm)
Control group	15.03 ± 2.62
TNTs group	62.83 ± 6.44**
minTBP-1-IGF-1 group	6.37 ± 2.14**
minTBP-1-IGF-1-TNTs group	14.31 ± 3.95

*$p < 0.05$, **$p < 0.01$, $n = 10$.

Table 2: Water contact angle of the four experimental groups

Group	Water contact angle (°)
Control group	76.2 ± 6.1
TNTs group	27.6 ± 3.2**
minTBP-1-IGF-1 group	25.2 ± 4.6**
minTBP-1-IGF-1-TNTs group	13.5 ± 2.7**

*$p < 0.05$, **$p < 0.01$, $n = 10$.

morphology was still visible even after protein adsorption. At low magnification, well-aligned and clean nanotubes can be seen on Ti surface after anodized oxidation (Figure 2(m)); moreover, the nanotubes have been completely covered by protein evenly after protein adsorption (Figure 2(n)). The roughness of the four groups revealing Ra (nm) values from Table 1 was 15.03 (control group), 62.83 (TNTs group), 6.37 (minTBP-1-IGF-1 group), and 14.31 (minTBP-1-IGF-1-TNTs group) in average, respectively.

3.2 Water contact angle test

The surface wettability of interface was characterized by water contact angle measurement. Water contact angle measurement results showed that surface wettability changed from 76.2 ± 6.1° (control group) to 27.6 ± 3.2° (TNTs group), 25.2 ± 4.6° (minTBP-1-IGF-1 group), and 13.5 ± 2.7° (minTBP-1-IGF-1-TNTs group), receptively. These results confirmed that the minTBP-1-IGF-1 and TNTs improved surface hydrophilicity (Figure 3) and the minTBP-1-IGF-1-TNTs surface showed the highest hydrophilicity (Table 2).

3.3 Assaying adsorbed modified IGF-1s

After immersion for 24 h, the densities of the minTBP-1-IGF-1 adsorbed on machined Ti surface (Table 3) were 587 ± 67 ng/cm^2, whereas the densities of minTBP-1-IGF-1 adsorbed on TNTs surface were 726 ± 58 ng/cm^2. But there was no significant difference between the 6 and 24 h protein adsorption on the two surfaces within group as shown in Figure 4. Therefore, the soaking time of the specimens in the protein solution was set at 6 h.

3.4 Construction of the type 2 diabetes model, IPGTT, and ITT

Throughout the experiment, the blood glucose level of the SD rats was stable at around 18.6 mmol/L after diabetes

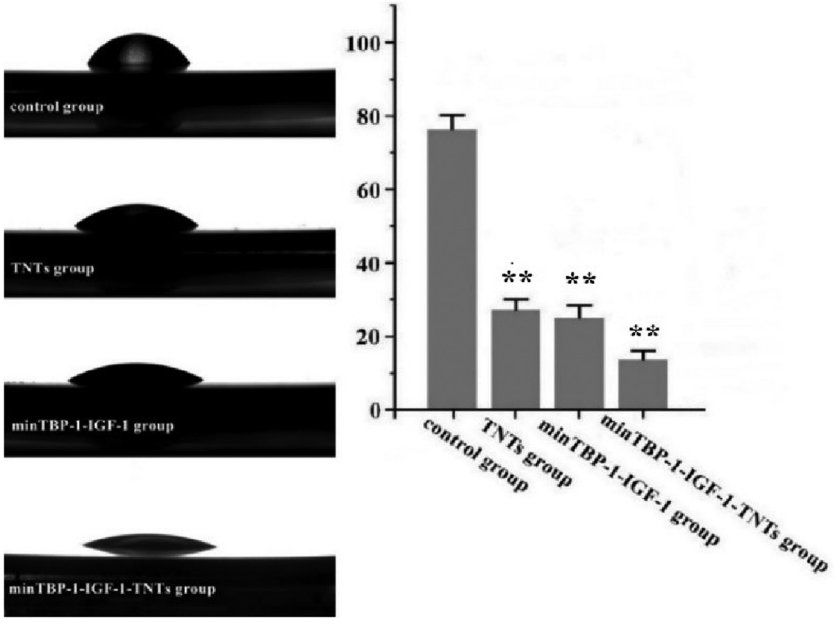

Figure 3: Water contact angle of the modified interfaces. *$p < 0.05$, **$p < 0.01$, $n = 10$.

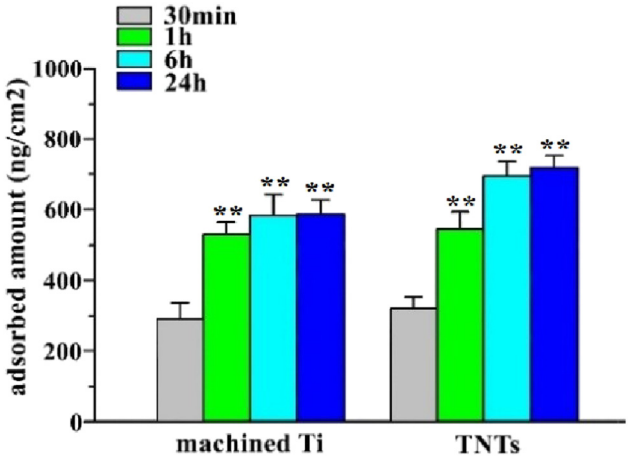

Figure 4: Amounts of adsorbed minTBP-1-IGF-1 on machined Ti surfaces and TNTs surface were estimated. *p < 0.05, **p < 0.01, n = 10.

Table 3: Amounts of adsorbed minTBP-1-IGF-1 on machined Ti surfaces and TNTs surface

Time	Machined Ti (ng/cm^2)	TNTs (ng/cm^2)
30 min	280.9 ± 45.8	312.9 ± 28.4
1 h	533.3 ± 39.0**	544.9 ± 51.0**
6 h	571.9 ± 72.4**	702.4 ± 47.2**
24 h	587.1 ± 67.4**	726.3 ± 58.5**

*p < 0.05, **p < 0.01, n = 10.

induction and their weight had significantly increased (Figure 5(e), Table 4).

For the purpose of analyzing glucose tolerance in each group, IPGTTs were performed. The plasma glucose increased to a maximum after 30 min of glucose administration i.p. in both normal and diabetic rats (Table 5), but this increase was higher in diabetic rats (p < 0.01) (Figure 5(a)). There was altogether delay of glucose clearance in diabetic rats, with glucose levels remaining elevated for 120 min (p < 0.01) after glucose administration. AUC (Figure 5(b)) of blood glucose during the IPGTT was more than twice as much as in normal rats (3245.4 *vs* 1452.0 mmol/L, _120 min in average, p < 0.001, Table 6), thereby qualifying for characterization as glucose intolerance.

To investigate the differences in insulin sensitivity, an ITT was performed. For ITT (Figure 5(c), Table 7), there was a rapid decline in plasma glucose up to 30 min of insulin administration in normal SD rats. But plasma glucose remained higher in diabetic rats (p < 0.01) at all time-points up to 120 min. The higher AUC (Figure 5(d)) was measured in T2DM rats than that in the normal rats (1835.3 *vs* 334.0 mmol/L, _120 min in average, p < 0.001, Table 6), characterizing the rats as insulin resistant.

The model rats had the characteristics of hyperglycemia and insulin resistance, which indicated that these rats were successfully modeled T2DM [4,6]. The micro-CT evaluation demonstrated that femurs of T2DM rats showed obvious osteoporosis (Figure 5(f)).

3.5 Measurement of MAR

Figure 6 shows fluorescence microscopic images of early bone formation around the implant. From Figure 6(d), the minTBP-1-IGF-1-TNTs group had the widest fluorescence spacing, followed by the minTBP-1-IGF-1 group (Figure 6(c)) and the TNTs group (Figure 6(b)), and the control group had the smallest spacing (Figure 6(a)). From Figure 5(e), the MAR value of the control group (Table 8) was the lowest (0.71 ± 0.19 μm/day), followed by the TNTs group (0.88 ± 0.22 μm/day) and the minTBP-1-IGF-1 group (1.27 ± 0.31 μm/day), and the highest was the minTBP-1-IGF-1-TNTs group (1.86 ± 0.39 μm/day).

3.6 *In vivo* micro-CT evaluation

The micro-CT reconstructed images (Figure 7(a)–(d)) clearly demonstrated the architectural changes in trabecular bone around the implant. At each time point, the thickness of the newly formed bone surrounding the implant was obviously denser and more homogeneous in the minTBP-1-IGF-1-TNTs group than those in the other groups. At the 12th week, the bone formed around the machined/TNTs/minTBP-1-IGF-1 implant was inconsistent and sparse, while the bone formed in the minTBP-1-IGF-1-TNTs group was continuous and dense. The BV/TV, Tb.Th, Tb.N, BS/BV, and Tb.Sp were quantified 12 weeks after implantation (Figure 7(e)–(i) and Table 9). Increase of BV/TV, Tb.Th, and Tb.N and decrease of BS/BV and Tb.Sp indicated vigorous bone growth. Among the four groups, the minTBP-1-IGF-1-TNTs group had the highest values in BV/TV, Tb.N, and Tb.Th, and the lowest values in BS/BV and Tb.Sp.

3.7 SEM/EDS analysis of cross-sections

The SEM micrographs (Figure 8) of cross-Section 4 and 8 weeks after implantation showed that in the control group (Figure 8a) there was clear gap between bone and implant. After being modified by TNTs (Figure 8b), minTBP-1-IGF-1 (Figure 8c), and minTBP-1-IGF-1-TNTs (Figure 8d), the gap

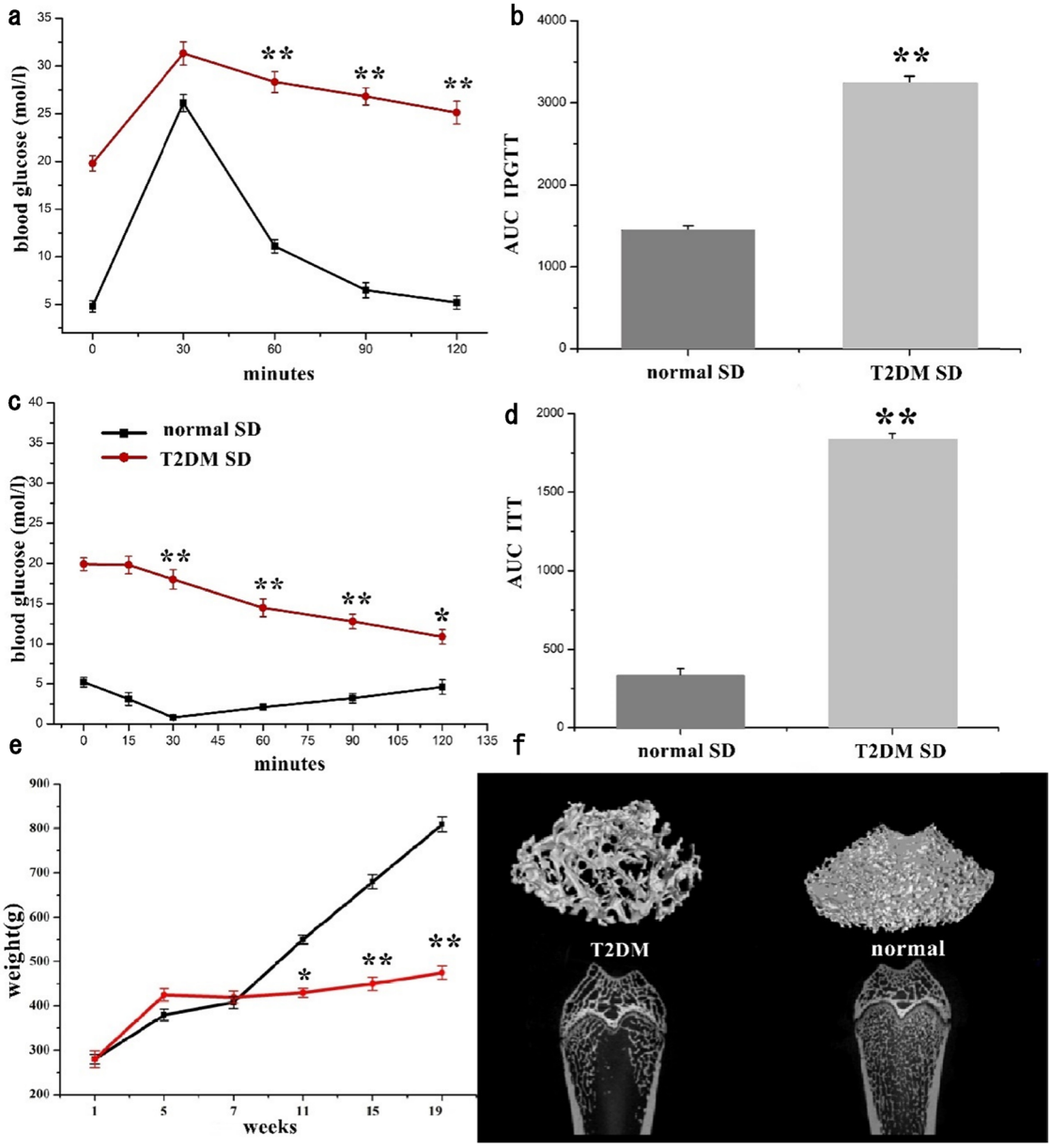

Figure 5: (a) Plasma glucose during IPGTT in rats 4 weeks after injection, (b) AUC of IPGTT assessment, (c) percentage of initial glucose level during ITT in T2DM and normal SD rats, (d) AUC of ITT assessment, (e) body weight changed with time from the beginning to the end of experiment, and (f) micro-CT scan of epiphysis of femoral shaft. *$p < 0.05$, **$p < 0.01$, $n = 6$.

Table 4: Body weight changed with time from the beginning to the end of experiment

Time (weeks)	Normal SD (g)	T2DM SD (g)
1	280 ± 11	280 ± 19
5	380 ± 13	425 ± 14
7	408 ± 14	420 ± 14
11	550 ± 10	430 ± 10*
15	680 ± 16	450 ± 15**
19	809 ± 17	475 ± 15**

*$p < 0.05$, **$p < 0.01$, $n = 6$.

Table 5: Plasma glucose during IPGTT in rats 4 weeks after injection

Time (min)	Normal SD (mol/L)	T2DM SD (mol/L)
0	4.8 ± 0.6	19.8 ± 0.8
30	26.1 ± 0.9	31.3 ± 1.2
60	11.1 ± 0.7	28.3 ± 1.1**
90	6.5 ± 0.8	26.8 ± 0.9**
120	5.2 ± 0.7	25.1 ± 1.2**

*$p < 0.05$, **$p < 0.01$, $n = 6$.

Table 6: AUC of IPGTT and ITT assessment

IPGTT		ITT	
Normal SD	**T2DM SD**	**Normal SD**	**T2DM SD**
1452.0 ± 49.9	3245.4 ± 79.5**	334.0 ± 41.3	1835.3 ± 38.1**

*p < 0.05, **p < 0.01, n = 6.

Table 7: Plasma glucose during ITT in rats 4 weeks after injection

Time (min)	Normal SD (mol/L)	T2DM SD (mol/L)
0	5.2 ± 0.6	19.9 ± 0.8
15	3.1 ± 0.8	19.8 ± 1.1
30	0.8 ± 0.2	18.0 ± 1.2**
60	2.1 ± 0.4	14.5 ± 1.1**
90	3.2 ± 0.6	12.8 ± 0.9**
120	4.6 ± 0.9	10.9 ± 0.9*

*p < 0.05, **p < 0.01, n = 6.

between the implant and bone became smaller. And it can be clearly seen that minTBP-1-IGF-1-TNTs group (Figure 8d) has the smallest gap between the implant and bone tissue.

Table 8: MAR was determined by a fluorescent microscope

Group	Water contact angle (°)
Control group	0.71 ± 0.19
TNTs group	0.88 ± 0.22
minTBP-1-IGF-1 group	1.27 ± 0.31**
minTBP-1-IGF-1-TNTs group	1.86 ± 0.39**

*p < 0.05, **p < 0.01, n = 6.

The SEM micrographs (Figure 9(a)–(d)) of cross-sections 12 weeks after implantation showed that in the control group there was clear gap between the bone and implant. After being modified by TNTs, minTBP-1-IGF-1, and minTBP-1-IGF-1-TNTs, the gap between the implant and bone became smaller. In particular, the bone and implant were in close contact with each other in the minTBP-1-IGF-1-TNTs group. The EDS analysis of the cross-section (Figure 9(f)–(i)) showed that contents of calcium and phosphor elements increased in order of the control group, the TNTs group, the minTBP-1-IGF-1 group, and the minTBP-1-IGF-1-TNTs group. The result of a linear element scanning across the bone–implant interface of the minTBP-1-IGF-1-TNTs group (Figure 9e) showed the enrichment of calcium, phosphorus, and oxygen ions at the interface.

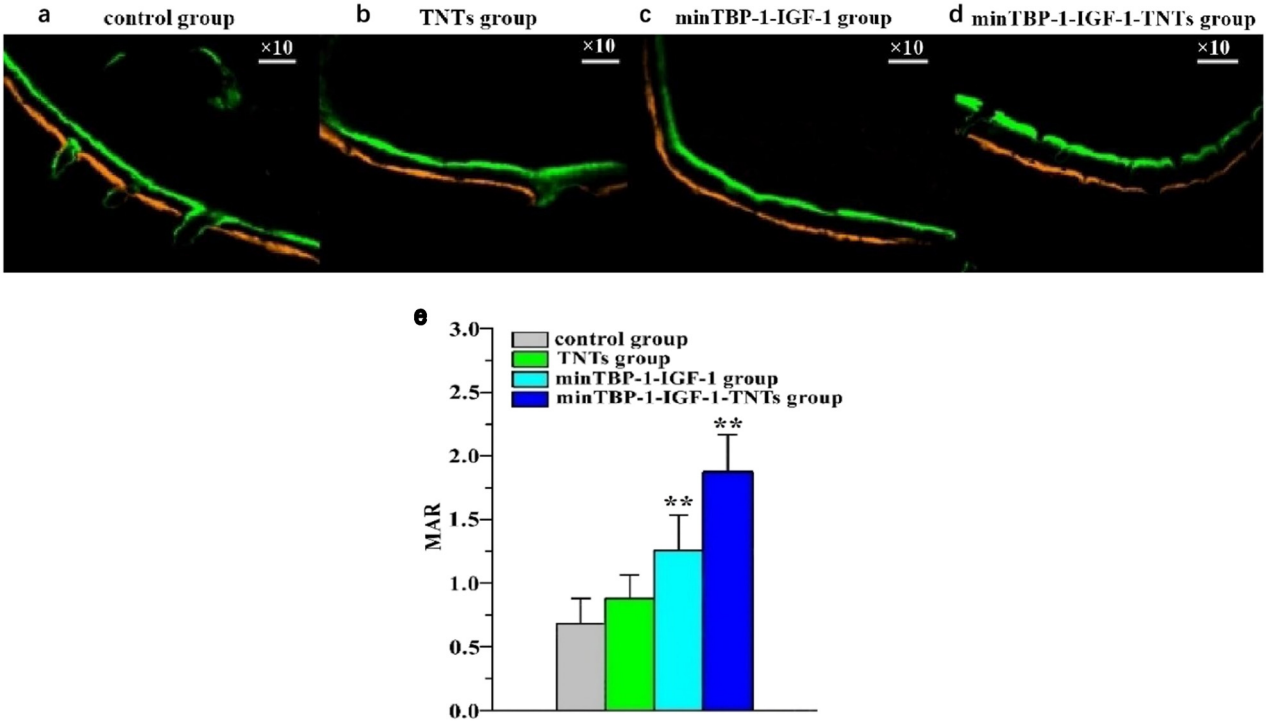

Figure 6: (a)–(d) Fluorescence microscopic images of bone formed around the implant after labeling with alizarin red (red) and calcitrin (green) at 4 and 8 weeks (magnification ×10). (e) MAR was determined by a fluorescent microscope; *p < 0.05, **p < 0.01, n = 6.

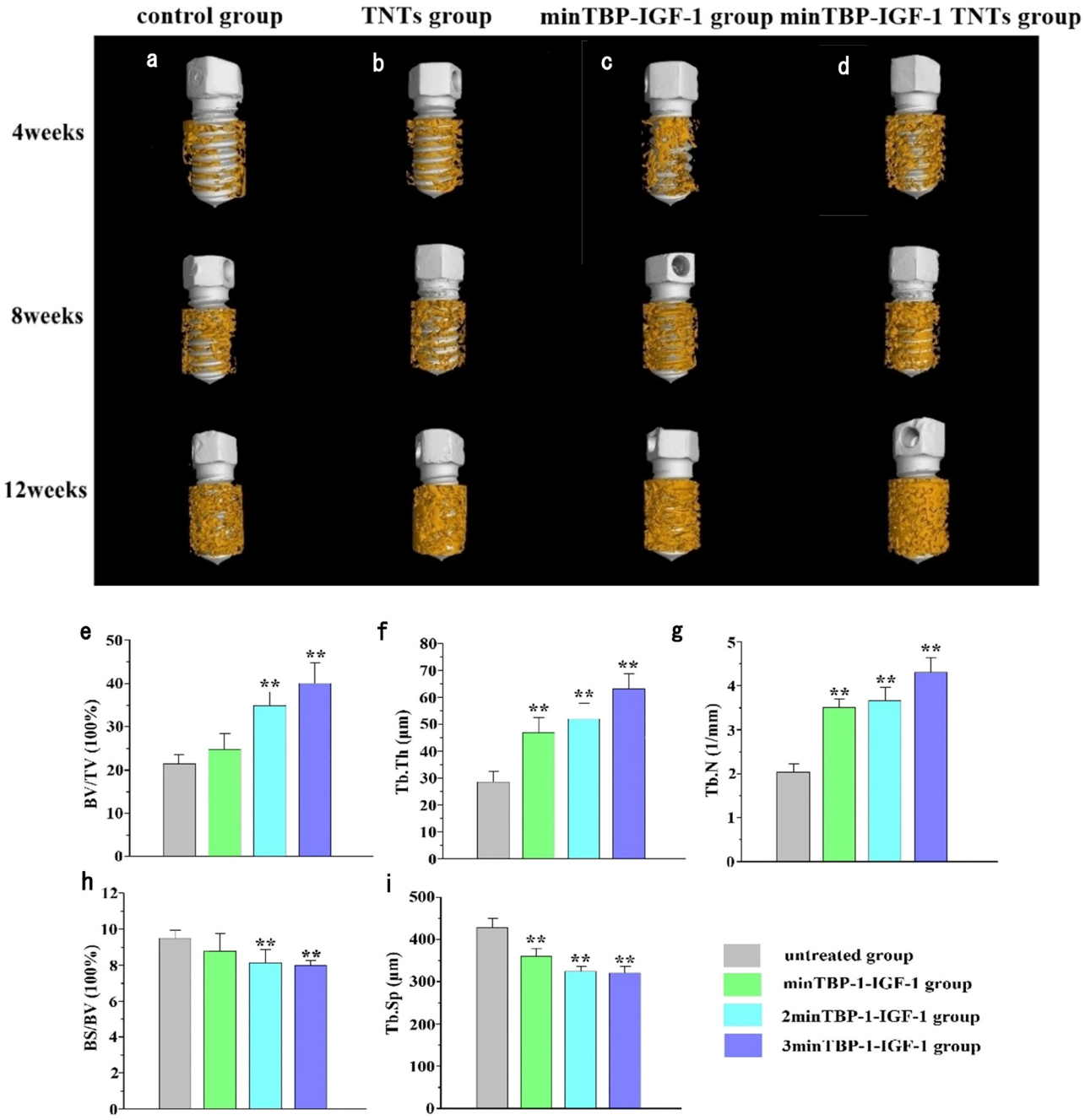

Figure 7: (a)–(d) Micro-CT images at 4, 8, and 12 weeks after implantation. (e)–(i) Micro-CT statistical analysis of BV/TV, Tb.Th, Tb.N, BS/BV, and Tb.Sp 12 weeks after implantation; *$p < 0.05$, **$p < 0.01$, $n = 6$.

Table 9: Micro-CT statistical analysis of BV/TV, Tb.Th, Tb.N, BS/BV, and Tb.Sp 12 weeks after implantation

Group	BV/TV	Tb.Th	Tb.N	BS/BV	Tb.Sp
Control group	21.7 ± 2.6	28.3 ± 4.7	2.1 ± 0.2	9.6 ± 0.4	423.2 ± 23.5
TNTs group	25.2 ± 4.1	46.7 ± 6.6**	3.5 ± 0.2**	8.9 ± 1.2	354.1 ± 21.3**
minTBP-1-IGF-1 group	34.8 ± 3.8**	51.2 ± 6.2**	3.7 ± 0.3**	8.1 ± 0.9**	319.5 ± 10.9**
minTBP-1-IGF-1-TNTs group	39.5 ± 4.9**	61.8 ± 7.3**	4.3 ± 0.4**	7.9 ± 0.3**	316.8 ± 19.8**

*$p < 0.05$, **$p < 0.01$, $n = 9$.

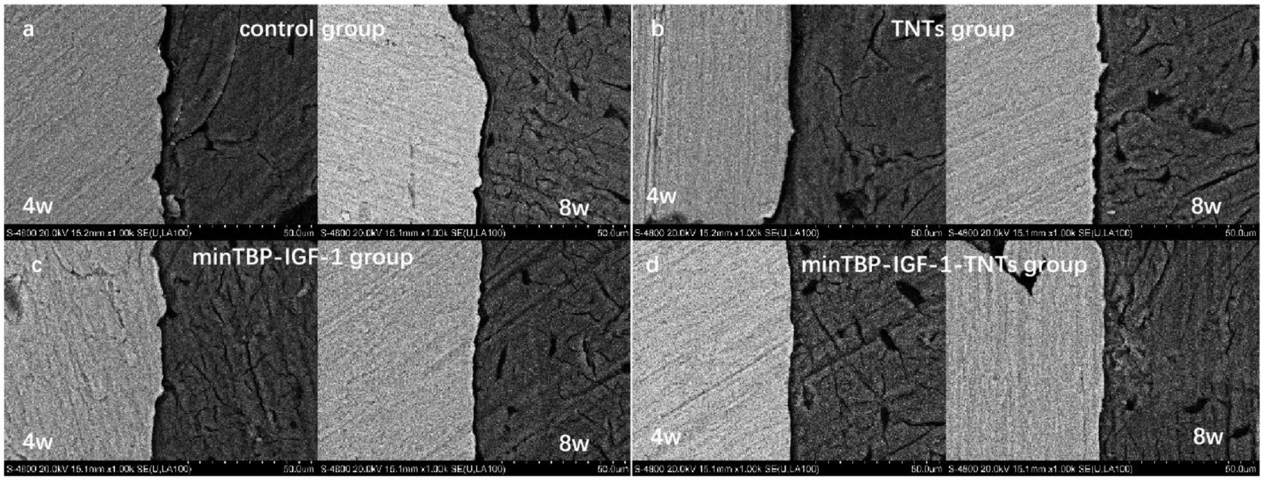

Figure 8: Cross-section SEM photomicrographs 4 and 8 weeks after implantation (n = 6).

4 Discussion

Despite the extensive use of titanium, and the considerably growing body of studies on the advancement of new titanium surfaces and/or modification of available surfaces, implant osseointegration in medically compromised patients still remains a challenge. T2DM is currently the quite common systemic disease affecting implant success [3]. T2DM is characterized by high blood glucose and insulin resistance. In this study, we established a T2DM rat model, which was confirmed to have the characteristics of hyperglycemia and insulin resistance by ITT and IGTT assay (Figure 5(a)–(d)). When normal and T2DM rats were injected with high glucose solution and insulin intraperitoneally, the blood glucose of the T2DM rats was significantly higher than that of the normal rats. The above results confirmed that we successfully prepared the T2DM rat model. In this study, we selected rats as research animals. The reasons are as follows: first, rats are cost-effective and easy to handle, second, its development process and anatomical structure are similar to those of human beings, third, the rat model allows standardized experimental procedure, and finally, the implantation was performed at the distal femur of rats, because there are a large number of cancellous bones, whose tissue structure is similar to that of human jaw, which is easy to operate and observe. At present, embedding the implant into the rat tibia for implant observation has been reported in many literature [3,4,28].

A growing body of evidence indicates that impaired osteoblast-mediated microstructure defects and poor bone quality by T2DM is the important reason for low osseointegration [3]. Our experiment also affirmed that osteoporosis occurred in T2DM rat through the micro-CT examination (Figure 5(f)). Because of the important role of IGF-1 in promoting osteoblast differentiation and mineralization under diabetic condition [25,26], we had prepared a recombinant minTBP-1-IGF-1 for improving implant osseointegration. MinTBP-1 is a TiO_2 specific nucleic acid aptamer, which has high affinity with TiO_2. Therefore, the recombinant protein can be automatically adsorbed on the implant surface. Through previous *in vitro* experiments, we confirmed that the recombinant protein can effectively play the biological function of IGF-1 [23]. In order to effectively increase the loading amount of the functional proteins, anodized TNTs were introduced as protein carriers. The preparation of TNTs layer can be easily integrated into the Ti and Ti-alloy implant to increase drug loading and sustained release [13]. The AFM and SEM images showed that the highly ordered TNTs were achieved and the nanotube windows were clean and open. Compared to the amount of the protein adsorbed on the Ti surface, the adsorption amount of fusion protein on the TNTs modified surface was greatly increased. The main reason was that TNTs have high ratio surface areas [13].

Wettability of the modified surface has been known as a significant factor to control the dynamic interactivity between implanted surface and blood or serum *in vivo* [29,30]. Osteoblasts do not directly interact with biomaterial surface, instead they interact with adsorbed proteins from blood or serum. Therefore, the surface with high hydrophilicity is conducive to protein adhesion and subsequent cell adhesion, spreading, and osteogenic expression [4,31]. The surface hydrophilicity from high to low was the minTBP-1-IGF-1-TNTs surface, the minTBP-1-IGF-1 surface, the TNTs surface, and the machined surface. Therefore, we speculated that because of the highest hydrophilicity, the

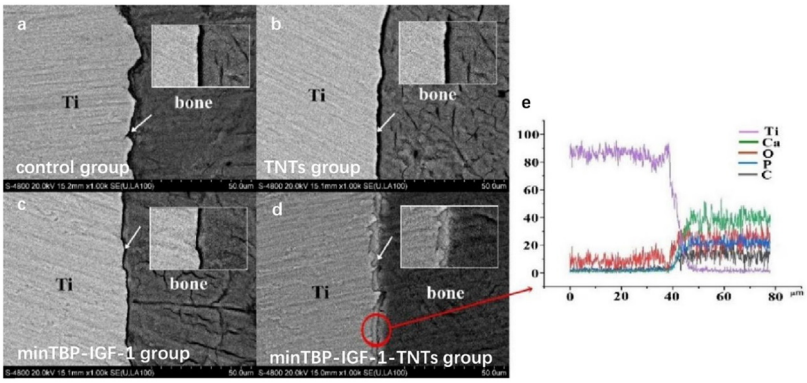

f control group

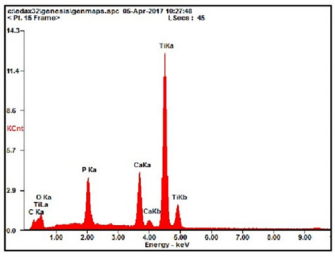

Element	Wt%	At%
CK	06.48	16.36
OK	16.23	30.77
PK	07.47	07.32
CaK	10.78	08.16
TiK	59.04	37.39
Matrix	Correction	ZAF

g TNTs group

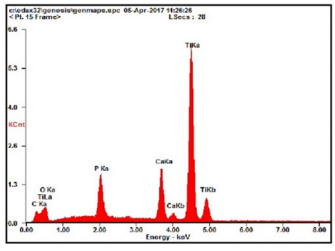

Element	Wt%	At%
CK	05.44	14.36
OK	14.08	27.91
PK	08.17	08.37
CaK	11.64	09.21
TiK	60.66	40.15
Matrix	Correction	ZAF

h minTBP-IGF-1 group

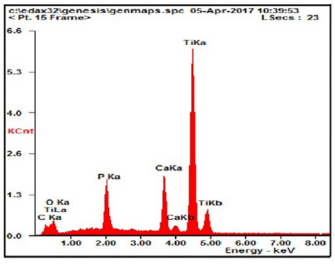

Element	Wt%	At%
CK	05.73	15.08
OK	13.81	27.30
PK	08.22	08.40
CaK	11.77	09.29
TiK	60.47	39.93
Matrix	Correction	ZAF

i minTBP-IGF-1-TNTs group

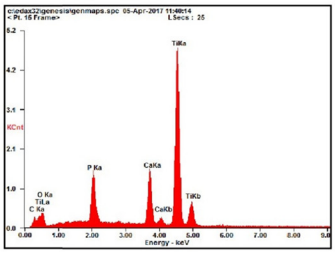

Element	Wt%	At%
CK	05.47	14.27
OK	14.75	28.91
PK	08.62	08.72
CaK	11.99	09.38
TiK	59.17	38.72
Matrix	Correction	ZAF

Figure 9: (a)–(d) Cross-section SEM photomicrographs, (e) line scan analysis of minTBP-1-IGF-1-TNTs group, and (f)–(i) EDS analysis of Ti–implant interfaces 12 weeks after implantation, $n = 6$.

minTBP-1-IGF-1-TNTs surface was best for osteoblast adhesion and spreading, and the subsequent formation and mineralization of bone tissue.

Osseointegration is a prerequisite for successful implant repair, and it often takes 3–6 months after implantation [32,33]. For oral implants, it has become the key to shorten the osseointegration cycle and improve the osseointegration rate by modifying the implant surface. Poor early osseointegration is considered to be one of the main reasons for implant failure [34]. Therefore, we observed the osseoinducibility in the early stage around the modified implants through observing the distance between the two fluorescent drugs. Previous studies have suggested that the bone-to-implant contact is impaired in patients with DM because the bone formed around implant is incomplete and delayed and the newly formed bone is immature and poorly organized [31,35,36]. It can be seen from Figure 6(a) that the fluorescence spacing of the two colors was the closest, indicating that the formation of bone tissue was the least. And it is clearly seen that the formation of early mineralized bone tissue in the minTBP-1-IGF-1-TNTs group (Figure 6(d)) was more than that in the TNTs group (Figure 6(b)) and the minTBP-1-IGF-1 group (Figure 6(c)), which was not only due to the preparation of nanotubes, but also due to the loading of recombinant IGF-1 on implant surface.

Osseointegration is the direct contact between living bone and the surface of a load-bearing synthetic implant, without the interposition of non-bone tissue. Since the direction of 2D slice around the central axis of the implant, the change of tissue morphology measurement is about 30–35%, so one slice of each sample is considered insufficient to fully determine the bone implant contact [37,38]. Micro-CT imaging is fast, non-destructive, and allows three-dimensional evaluation. Butz *et al.* [39] compared the correlation between micro-CT and histological imaging for cortical and cancellous bones at distances of 0–24, 24–80, 80–160, and 160–240 μm from the implant surface. It also confirmed that this method has revealed to be a feasible alternative to current bone regeneration quantification methods [40]. In order to confirm the effect of different modification methods on the whole period of implant osseointegration, we used micro-CT for qualitative and quantitative analysis. It has been confirmed that the structure and morphology of nanotubes can promote the early response of osteoblasts and facilitate the early bone formation around implants [1,11]. The micro-CT results (Figure 7(a) and (b)) showed that the TNTs modified implant could improve the implant osseointegration under T2DM condition. However, compared with the TNTs group, the bone formed around the implant in the minTBP-1-IGF-1 group and the minTBP-1-IGF-1-TNTs group (Figure 7(c) and (d)) from 4 to 12 weeks was more abundant. The highest value of BV/TV, Tb.Th, and Tb.N and the lowest value of BS/BV and Tb.Sp also confirmed that the most bone tissue was formed around the implant in the minTBP-1-IGF-1-TNTs group (Figure 7(e)–(i)). Tb.Sp value is related to the stability of bone volume around the implant and a high Tb.Sp value demonstrates that bone resorption is more likely to occur around the implant [2]. Among all groups, the minTBP-1-IGF-1-TNTs group had the lowest Tb.Sp value, which indicated that the combination of minTBP-1-IGF-1 and TNTs can effectively enhance the bone maintenance around the implant. In humans, IGF-1 and its binding proteins have positive roles in the acquisition of peak bone mass and the maintenance of bone mineral density [14]. Reduced expression of IGF-I resulted in attenuation of the bone mineralization in diabetic rats and low circulating levels of IGF-1 are associated with osteoporosis and fracture [15,16]. Numerous studies have highlighted the potential of IGF-1 to induce bone regeneration; local administration of IGF-1 has been shown to augment new bone formation and promote bridging bone defects *in vivo* [41,42]. In this study, it was confirmed that the effect of combined use of minTBP-1-IGF-1 and TNTs in promoting osteogenesis was significantly better than that of minTBP-1-IGF-1 or TNTs alone, and TNTs can be used as an effective carrier of minTBP-1- IGF-1. It can also be confirmed from the cross-section SEM of the implant and bone that the implant in the minTBP-1-IGF-1-TNTs group had the closest cohesion to the bone tissue (Figures 8 and 9), and the EDS scanning that hydroxyapatite was formed on the contact surface (Figure 9). Although the analysis of SEM and EDS in this section was qualitative, both indicated that the minTBP-1-IGF-1-TNTs group can effectively promote the formation of bone tissue around the implant in T2DM condition.

5 Conclusion

Low implant osseointegration under T2DM condition is a thorny problem in clinical practice. While the minTBP-1-IGF-1-TNTs is a brand-new method to solve this problem, which is not only effectively enhancing the bone formation around the implant in the short term, but also significantly improving the long-term osseointegration.

Funding information: This work was supported by Shaanxi Natural Science Foundation of China (No. S2020-YF-YBSF-0432) and Shaanxi Science and Technology Innovation Team Project (No. 2021TD-46).

Author contributions: All authors have accepted responsibility for the entire content of this manuscript and approved its submission.

Conflict of interest: The authors state no conflict of interest.

Ethical approval: The research related to animals' use has been complied with all the relevant national regulations and institutional policies for the care and use of animals.

References

[1] Yang J, Zhang H, Chan SM, Li R, Wu Y, Cai M, et al. TiO_2 nanotubes alleviate diabetes-induced osteogenetic inhibition. Int J Nanomed. 2020;15:3523–37. doi: 10.2147/IJN.S237008.

[2] Tan N, Liu X, Cai Y, Zhang S, Jian B, Zhou Y, et al. The influence of direct laser metal sintering implants on the early stages of osseointegration in diabetic mini-pigs. Int J Nanomed. 2017;12:5433–42. doi: 10.2147/IJN.S138615.

[3] Zhang J, Wang Y-N, Jia T, Huang H, Zhang D, Xu X. Genipin and insulin combined treatment improves implant osseointegration in type 2 diabetic rats. J Orthop Surg Res. 2021;16:59–69. doi: 10.1186/s13018-021-02210-1.

[4] Wang B, Song Y, Wang F, Li D, Zhang H, Ma A, et al. Effects of local infiltration of insulin around titanium implants in diabetic rats. Br J Oral Maxillofac Surg. 2021;9:225–9. doi: 10.1016/j.bjoms.2010.03.006.

[5] Alshahrani A, Al Deeb M, Alresayes S, Mokeem SA, Al-Hamoudi N, Alghamdi O, et al. Comparison of peri-implant soft tissue and crestal bone status of dental impla nts placed in prediabetic, type 2 diabetic, and non-diabetic individuals: a retrospective cohort study. Int J Implant Dent. 2020;6:56–63. doi: 10.1186/s40729-020-00255-1.

[6] Huang H, Luo L, Liu Z, Li Y, Tong Z, Liu Z. Role of TNF-α and FGF-2 in the fracture healing disorder of type 2 diabetes model induced by high fat diet followed by streptozotocin. Diabetes Metab Syndr Obes. 2020;13:2279–88. doi: 10.2147/DMSO.S231735.

[7] Chen B, He Q, Yang J, Pan Z, Xiao J, Chen W, et al. Metformin suppresses oxidative stress induced by high glucose via activation of the Nrf2/HO-1 signaling pathway in type 2 diabetic osteoporosis. Life Sci. 2022;312:121092. doi: 10.1016/j.lfs.2022.121092.

[8] Jia T, Wang YN, Feng Y, Wang C, Zhang D, Xu X. Pharmic activation of PKG2 alleviates diabetes-induced osteoblast dysfunction by suppressing PLCβ1-Ca^{2+}-mediated endoplasmic reticulum stress. Oxid Med Cell Longev. 2021;2021:5552530. doi: 10.1155/2021/5552530.

[9] Oliveira PGFP, Coelho PG, Bergamo E, Witek L, Borges CA, Bezerra FB, et al. Histological and nanomechanical properties of a new nanometric hydroxiapatite implant surface: an *in vivo* study in diabetic rats. Materials. 2020;13:5693–709. doi: 10.3390/ma13245693.

[10] Novaes AB Jr, Souza SLSD, de Barros RR, Pereira KK, Iezzi G, Piattelli A. Influence of implant surfaces on osseointegration. Braz Dent J. 2021;21:471–81. doi: 10.1590/S0103-64402010000600001.

[11] Awad NK, Edwards SL, Morsi YS. A review of TiO_2 NTs on Ti metal: electrochemical synthesis, functionalization and potential use as bone implants. Mater Sci Eng C Mater Biol Appl. 2017;76:1401–12. doi: 10.1016/j.msec.2017.02.150.

[12] Huang J, Zhang X, Yan W, Chen Z, Shuai X, Wang A, et al. Nanotubular topography enhances the bioactivity of titanium implants. Nanomedicine. 2017;13:1913–23. doi: 10.1016/j.nano.2017.03.017.

[13] Park J, Cimpean A. Anodic TiO2 nanotubes: tailoring osteoinduction via drug delivery. Nanomaterials. 2021;11:2359–99. doi: 10.3390/nano11092359.

[14] Oh S, Brammer KS, Li YS, Teng D, Engler AJ, Chien S, et al. Stem cell fate dictated solely by altered nanotube dimension. Proc Natl Acad Sci. 2019;106:2130–5. doi: 10.1073/pnas.0813200106.

[15] Gulati K, Ramakrishnan S, Aw MS, Atkins GJ, Findlay DM, Losic D. Biocompatible polymer coating of titania nanotube arrays for improved drug elution and osteoblast adhesion. Acta Biomater. 2012;8:449–56. doi: 10.1016/j.actbio.2011.09.004.

[16] Losic D, Simovic S. Self-ordered nanopore and nanotube platforms for drug delivery applications. Expert Opin Drug Deliv. 2009;6:1363–81. doi: 10.1517/17425240903300857.

[17] Wang D, Mao J, Zhou B, Liao XF, Gong SQ, Liu Y, et al. A chimeric peptide that binds to titanium and mediates MC3T3-E1 cell adhesion. Biotechnol Lett. 2011;33:191–7. doi: 10.1007/s10529-010-0411-9.

[18] Gulati K, Santos A, Findlay D, Losic D. Optimizing anodization conditions for the growth of titania nanotubes on curved surfaces. J Phys Chem C. 2015;119:16033–45. doi: 10.1021/acs.jpcc.5b03383.

[19] Losic D, Aw MS, Santos A, Gulati K, Bariana M. Titania nanotube arrays for local drug delivery: recent advances and perspectives. Expert Opin Drug Deliv. 2015;12:103–27. doi: 10.1517/17425247.2014.945418.

[20] Kawai M, Rosen CJ. The insulin-like growth factor system in bone: Basic and clinical implications. Endocrinol Metab Clin N Am. 2012;41:323–33. doi: 10.1016/j.ecl.2012.04.013.

[21] Sheng MH, Lau KH, Baylink DJ. Role of osteocyte-derived insulin-like growth factor I in developmental growth, modeling, remodeling, and regeneration of the bone. J Bone Metab. 2014;21:41–54. doi: 10.11005/jbm.2014.21.1.41.

[22] Niu T, Rosen CJ. The insulin-like growth factor-I gene and osteoporosis: A critical appraisal. Gene. 2005;361:38–56. doi: 10.1016/j.gene.2005.07.016.

[23] Sano K, Shiba K. A hexapeptide motif that electrostatically binds to the surface of titanium. J Am Chem Soc. 2003;125:14234–5. doi: 10.1021/ja038414q.

[24] Sano K, Sasaki H, Shiba K. Specificity and biomineralization activities of Ti-binding peptide-1 (TBP-1). Langmuir. 2005;21:3090–5. doi: 10.1021/la047428m.

[25] Hayashi T, Sano K, Shiba K, Kumashiro Y, Iwahori K, Yamashita I, et al. Mechanism underlying specificity of proteins targeting inorganic materials. Nano Lett. 2006;6:515–9. doi: 10.1021/nl060050n.

[26] Zhang Q, Wang J, Cheng. B. The effects of functionalized titanium with minTBP-1-IGF-1 for improving osteoblast activity. Mater Lett. 2018;227:58–61. doi: 10.1016/j.matlet.2018.05.005.

[27] Berglundh T, Stavropoulos A, Working Group 1 of the VIII European Workshop on Periodontology. Preclinical *in vivo* research in implant dentistry. Consensus of the eighth European workshop on periodontology. J Clin Periodontol. 2012;39(Suppl 12):1–5. doi: 10.1111/j.1600-051X.2011.01827.x.

[28] Sohrabipour S, Sharifi MR, Talebi A, Sharifi M, Soltani N. GABA dramatically improves glucose tolerance in streptozotocin-induced

diabetic rats fed with high-fat diet. Eur J Pharmacol. 2018;826:75–84. doi: 10.1016/j.ejphar.2018.01.047.
[29] Nath S, Ghosh SK, Choudhury Y. A murine model of type 2 diabetes mellitus developed using a combination of high fat diet and multiple low doses of streptozotocin treatment mimics the metabolic characteristics of type 2 diabetes mellitus in humans. J Pharmacol Toxicol Met. 2017;84:20–30. doi: 10.1016/j.vascn.2016.10.007.
[30] Choee JH, Lee SJ, Lee YM, Rhee JM, Lee HB, Khang G. Proliferation rate of fibroblast cells on polyethylene surfaces with wettability gradient. J Appl Polym Sci. 2004;92:599–606. doi: 10.1002/app.20048.
[31] Gittens RA, Scheideler L, Rupp F, Hyzy SL, Geis-Gerstorfer J, Schwartz Z, et al. A review on the wettability of dental implant surfaces II: biological and clinical aspects. Acta Biomater. 2014;10:2907–18. doi: 10.1016/j.actbio.2014.03.032.
[32] Zhu X, Chen J, Scheideler L, Reichl R, Geis-Gerstorfer J. Effects of topography and composition of titanium surface oxides on osteoblast responses. Biomaterials. 2004;25:4087–103. doi: 10.1016/j.biomaterials.2003.11.011.
[33] Smeets R, Stadlinger B, Schwarz F, Beck-Broichsitter B, Jung O, Precht C, et al. Impact of dental implant surface modifications on osseointegration. Biomed Res Int. 2016;628:5620. doi: 10.1155/2016/6285620.
[34] Schwarz F, Derks J, Monje A, Wang H-L. Peri-implantitis. J Clin Periodontol. 2018;45(Suppl 20):S246–66. doi: 10.1111/jcpe.12954.
[35] Ruppa F, Liang L, Geis-Gerstorfer J, Scheideler L, Hüttig F. Surface characteristics of dental implants: a review. Dent Mater. 2018;34:40–57. doi: 10.1016/j.dental.2017.09.007.
[36] Gulati K, Aw MS, Findlay D, Losic D. Local drug delivery to the bone by drug-releasing implants: perspectives of nano-engineered titania nanotube arrays. Ther Deliv. 2012;3:857–73. doi: 10.4155/tde.12.66.
[37] Bissinger O, Probst FA, Wolff K-D, Jeschke A, Weitz J, Deppe H, et al. Comparative 3D micro-CT and 2D histomorphometry analysis of dental implant osseointegration in the maxilla of minipigs. J Clin Periodontol. 2017;44:418–27. doi: 10.1111/jcpe.12693.
[38] Hong JM, Kim UG, Yeo IL. Comparison of three-dimensional digital analyses and two-dimensional histomorphometric analyses of the bone–implant interface. PLoS One. 2022;10:e0276269. doi: 10.1371/journal.pone.0276269.
[39] Butz F, Ogawa T, Chang TL, Nishimura I. Three-dimensional bone–implant integration profiling using micro-computed tomography. Int J Oral Maxillofac Implant. 2006;1:687–95. doi: 10.1016/j.ijom.2006.03.021.
[40] Clozza E, Obrecht M, Dard M, Coelho PG, Dahlin C, Engebretson SP. A novel three-dimensional analysis of standardized bone defects by means of confocal scanner and micro-computed tomography. Clin Oral Investig. 2014;18:1245–50. doi: 10.1007/s00784-013-1081-5.
[41] Ashpole NM, Herron JC, Estep PN, Logan S, Hodges EL, Yabluchanskiy A, et al. Differential effects of IGF-1 deficiency during the life span on structural and biomechanical properties in the tibia of aged mice. AGE. 2016;38:38–51. doi: 10.1007/s11357-016-9902-5.
[42] Menendez LG, Sadaba MC, Puche JE, Lavandera JL, Castro LF, Gortazar AR, et al. IGF-I increases markers of osteoblastic activity and reduces bone resorption via osteoprotegerin and RANK-ligand. J Transl Med. 2013;11:271–82. doi: 10.1186/1479-5876-11-271.